Academic Journal of Science and Technology
ISSN: 2771-3032 | Vol. 20, No. 1, 2026

Optimization Design of Linear Variable Reluctance Resolver Structure Based on Kriging Surrogate Model

Zhenbing Fan [1], Yaohui Li [2]

[1] School of Information and Control Engineering, Jilin University of Chemical Technology, Jilin, Jilin, 132022, China
[2] School of Electromechanical Engineering, Xuchang University, Xuchang, Henan, 461000, China

Abstract: With the rapid development of high-end CNC machine tools and gravity energy storage technologies, long-stroke linear motion systems impose higher requirements on the measurement accuracy, reliability, and environmental adaptability of position sensors. Traditional optical and magnetic grating sensors are susceptible to interference in harsh conditions such as oil contamination and suffer from high costs and difficult maintenance. The Linear Variable Reluctance Resolver (LVRR) has become a potential ideal alternative due to its robust structure, strong anti-interference ability, and low cost. However, the "longitudinal end effect" and air-gap magnetic field distortion caused by extending the rotary structure to a linear one severely deteriorate the sinusoidal quality of the output signal, making it difficult for position resolution accuracy to meet high-precision control demands. To address this, this paper proposes an efficient structural optimization method combining Finite Element Analysis (FEA), the Kriging surrogate model, and the Expected Improvement (EI) criterion. By constructing a global Kriging surrogate model with mover end-tooth thickness, air-gap length, and slot depth as design variables and minimizing the Total Harmonic Distortion (THD) as the objective, the method employs a sequential iterative strategy to dynamically balance local exploitation and global exploration in the design space. Simulation results show that this method effectively suppresses end leakage flux and high-order harmonics. After optimization, the THD of the sensor's output voltage is reduced from 5.32% to 2.14%, and the peak electrical angle error converges to within $\pm0.9^\circ$, significantly improving the system's linearity and detection accuracy.

Keywords: Linear Variable Reluctance Resolver; End Effect; Kriging Surrogate Model; Total Harmonic Distortion; Finite Element Analysis.

1. Introduction

1.1. Research Background and Significance

In the context of "Industry 4.0" and "Made in China 2025", linear drive technology, with its efficient "zero-transmission" characteristics, is widely used in fields such as CNC machine tools, semiconductor lithography machines, rail transit, and gravity energy storage systems. The position detection system is the core for realizing high-precision closed-loop control, and its feedback accuracy, response speed, and environmental adaptability directly affect system motion performance.

Currently, linear displacement detection mainly employs linear encoders (optical and magnetic) and inductosyns. Optical encoders offer high accuracy but are sensitive to environmental cleanliness and easily affected by contamination; magnetic encoders have stronger contamination resistance but are susceptible to strong magnetic interference and are costly. The variable reluctance resolver (VRR), as a sensor based on the variable reluctance principle and long-term industrial validation, is recognized as a highly reliable angular sensor[6]. Extending its technical advantages to the field of linear position detection and developing a linear variable reluctance resolver (LVRR) holds significant engineering and economic value for reducing costs and enhancing reliability in harsh environments. [4,5]

1.2. Key Technical Challenges

Improving LVRR accuracy is key to enhancing linear motor performance. The process of geometrically stretching the closed circular magnetic circuit and periodically symmetric magnetic field distribution of rotary machines into a linear configuration inevitably introduces discontinuities in the linear motor mover's motion. This abrupt geometric change readily induces severe "longitudinal edge effects," leading to phenomena such as divergence of magnetic flux lines at the ends, local magnetic saturation, and non-sinusoidal distribution of the air-gap magnetic field[1,7]. Furthermore, the slotting effect also generates significant 3rd and 5th harmonic components in the air-gap permeance, which are primary factors causing nonlinear distortion in the induced electromotive force. This nonlinear distortion further exacerbates periodic errors in the mover's position information (obtained via the arctangent algorithm). Therefore, the core challenge in improving LVRR accuracy lies in how to reasonably optimize the structure to suppress edge effects and improve the air-gap magnetic field waveform[8,9].

2. LVRR Working Principle and Modeling Analysis

This study is based on a 3-pole-pair, 12-slot variable reluctance resolver (VRR) structure. This structure offers advantages such as simple and reasonable pole-slot combination, mature manufacturing process for signal windings, and stable fundamental magnetic field characteristics. The structural design of the linear variable reluctance resolver (LVRR) is realized by mapping the periodic structure from the cylindrical coordinate system of the rotary machine, unfolding it along the axial direction, and mapping it to the corresponding Cartesian coordinate system of the linear machine.

2.1. LVRR Structure

This study is based on a 3-pole-pair, 12-slot variable reluctance resolver (VRR) structure. This structure offers advantages such as simple and reasonable pole-slot combination, mature manufacturing process for signal windings, and stable fundamental magnetic field characteristics. The structural design of the linear variable reluctance resolver (LVRR) is realized by mapping the periodic structure from the cylindrical coordinate system of the rotary machine, unfolding it along the axial direction, and mapping it to the corresponding Cartesian coordinate system of the linear machine.

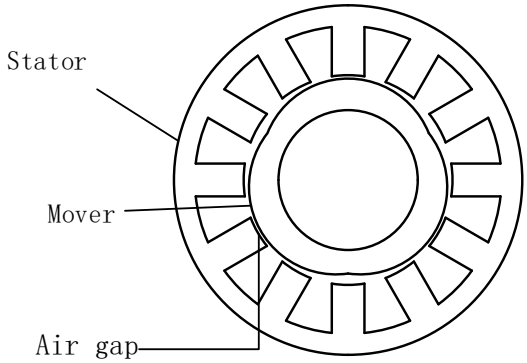

Fig 1. Structure diagram of a 3-pole-pair, 12-slot resolver

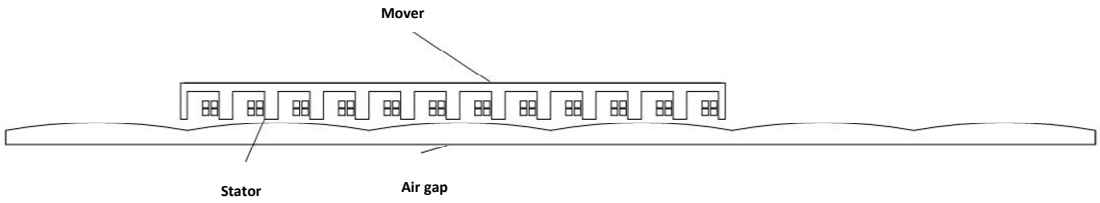

Fig 2. Model structure diagram of the linear variable reluctance resolver

2.2. Working Principle

The linear variable reluctance resolver shares the same electrical principle as the variable reluctance resolver, as shown in Fig. 3. The LVRR consists of a mover and a stator. The mover has two types of orthogonal windings on its inner side: an excitation winding whose axis is aligned with the direction of motion, and sine/cosine output windings whose axes are orthogonal to it. When an AC excitation voltage is applied to the excitation winding, induced electromotive forces (EMFs) are generated in the sine and cosine output windings due to electromagnetic coupling. The amplitude of these EMFs has a sine/cosine functional relationship with the linear displacement of the mover, enabling the conversion of mechanical position information into electrical signals.

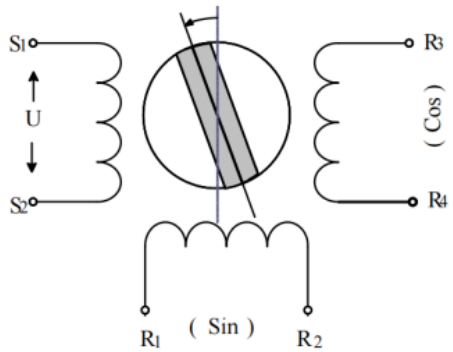

Fig 3. Working principle diagram of the linear variable reluctance resolver

2.3. Finite Element Model Construction

To accurately analyze the electromagnetic characteristics of the Linear Variable Reluctance Resolver (LVRR), this study first completed the two-dimensional (2D) geometric modeling in AutoCAD based on the parameters listed in Table 1. The geometry was subsequently imported into the MAGNET software to generate the LVRR structural model for simulation analysis (Fig. 4).

To balance computational accuracy and efficiency, a discretized mesh strategy was implemented for the LVRR. In critical regions with high magnetic field gradients, such as the air gap and tooth tips, a fine mesh of 0.5 mm was applied to precisely capture the magnetic field harmonic distribution and edge effects. Conversely, in the conjugate regions of the stator and mover where magnetic field variations are relatively smooth, a sparse mesh of 1.0 mm was utilized. The resulting global mesh configuration is illustrated in Fig. 5.

Subsequently, material properties and motion boundary conditions were defined. Both the mover and stator core materials were assigned as DW310-35 cold-rolled silicon steel. To approximate the actual operating conditions, the mover and a portion of the air gap were designated as moving components[9]. The motion type was defined as "speed-based" along the longitudinal direction of the stator, with a constant velocity of 5 m/s.

Finally, the solver configurations were established. A 2D transient motion field analysis was conducted with a total simulation duration of 20 ms. The time step was set to 0.00625 ms to ensure sufficient resolution of the dynamic processes under an excitation frequency of 10 kHz.

Table 1. Model parameters of the linear variable-reluctance resolver.

Parameter Name	Value
Rated Voltage / V	10 V
Rated Frequency / Hz	10 kHz
Rated Speed / ($r \cdot min^{-1}$)	1000
Number of Stator Slots	12
Number of Rotor Poles	6
Mover Length / mm	126.6
Stator Length / mm	253.2
Air Gap Length / mm	0.5
Mover/Stator Thickness / mm	10
Mover Tooth Length / mm	11.25
Mover Tooth Width / mm	3.1484

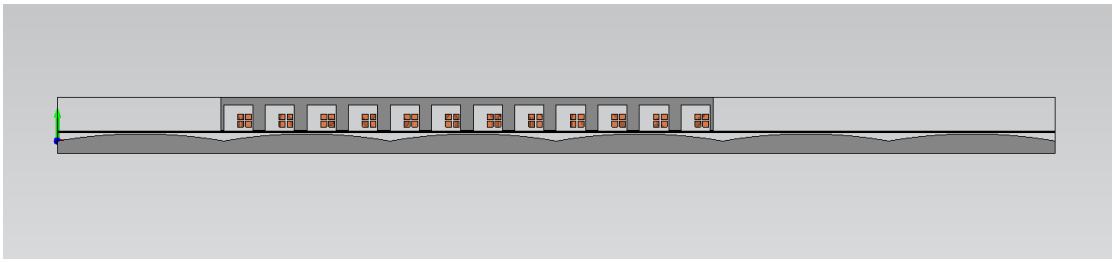

Fig 4. 2D structural diagram of the linear variable reluctance resolver

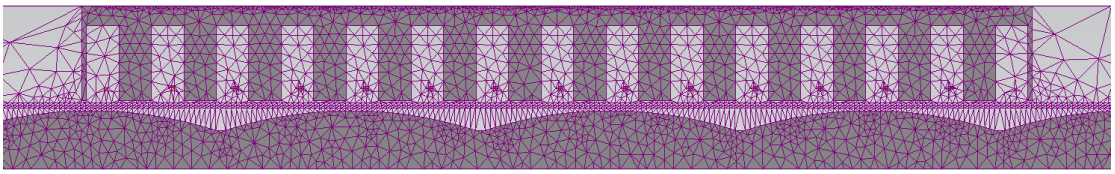

Fig 5. Finite element mesh distribution map

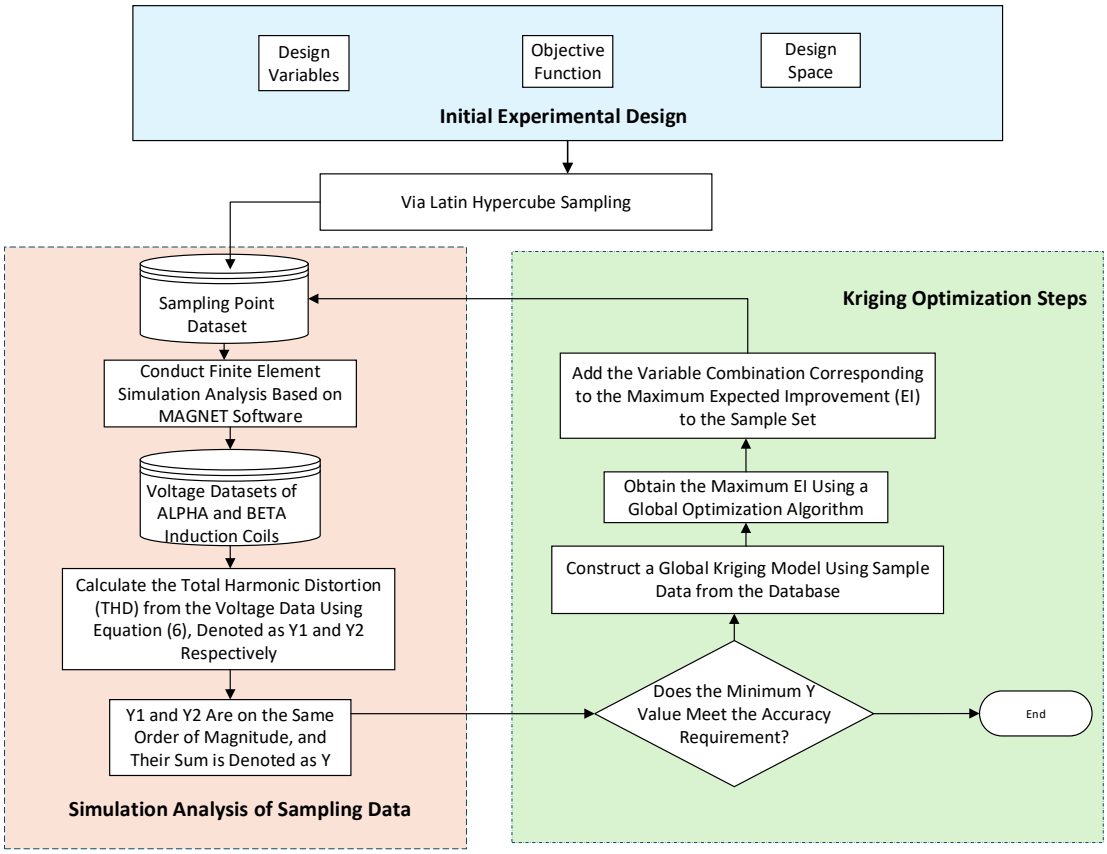

Fig 6. Global optimization flow chart based on the Kriging surrogate model

3. Optimization Design Method Based on the Kriging Model

Addressing the longitudinal end effects caused by the open-circuit structure of the Linear Variable Reluctance Resolver (LVRR) and the resulting output signal distortion, this study proposes a novel structural optimization method. This approach integrates Latin Hypercube Sampling (LHS), the Kriging surrogate model, and the Efficient Global Optimization (EGO) strategy[2,3]. By constructing a high-precision approximation model within local optimal regions to replace computationally intensive finite element simulations, the method enables the rapid and accurate optimization of structural parameters.

3.1. Optimization Variables and Objective Function

The mover end-tooth geometry, slot depth, and air gap geometric parameters are the critical factors inducing longitudinal end effects and subsequent distortion of the air gap magnetic flux density waveform [7]. To balance the degree of magnetic circuit saturation with signal sinusoidality, the following three key parameters are selected as design variables:

Mover end-tooth thickness (h_a): This parameter directly influences the intensity of end effects by altering the distribution of the end-leakage flux path. Its value range is set as$[0,4]$mm

Air gap length (δ): This determines the primary reluctance of the magnetic circuit and the harmonic content of the magnetic field. Its value range is set as $[0.3,1.0]$mm

Mover slot depth (h_d): This affects the magnetic circuit saturation by adjusting the saliency ratio of the mover. Its value range is set as $[2,7]$mm.

Here is the refined academic translation. I have formatted the THD formula into standard LaTeX for a professional research paper appearance.

The optimization objective is to minimize the Total Harmonic Distortion (THD) of the output voltage. The THD is calculated according to Equation (1):

$$\min f(x) = THD = \frac{\sqrt{\sum_{n=2}^{10} U_n^2}}{U_1} \times 100\% \quad (1)$$

Since the amplitude attenuation of higher-order harmonics has a negligible impact on position decoding errors, the THD calculation is truncated at the 10th harmonic.

3.2. Optimization Procedure and Modeling Strategy

As illustrated in Fig. 5, the proposed optimization design procedure is divided into three primary stages: initial experimental design and sampling, finite element simulation analysis, and Kriging model iterative optimization.

(1) Initial Experimental Design and Sampling

First, the design space, variables, and objective functions are defined. Subsequently, Latin Hypercube Sampling (LHS) is employed to generate uniformly distributed initial sampling points across the entire design domain.

(2) Finite Element Simulation Analysis

The sampling point data are imported into the MAGNET software to establish a 2D transient magnetic field model for finite element analysis (FEA). The induced electromotive force (EMF) data from the induction coils are extracted, and the THD_{sin} and THD_{cos} for each sampling point are calculated via FFT analysis. To ensure consistency in the multi-objective evaluation, THD_{sin} and THD_{cos} are normalized to the same order of magnitude and summed to obtain the total objective value, $F(x)$ thereby forming the initial sample database.

(3) Iterative Optimization Based on the Kriging Model

Model Construction: The data from the sample database are used to construct a global Kriging surrogate model that characterizes the mapping relationship between the design variables and the THD.

Global Optimization and EI Enhancement: An Efficient Global Optimization (EGO) strategy is adopted, utilizing a global optimization algorithm to search for the maximum point of the Expected Improvement (EI) function on the surrogate model.

Sample Update: The combination of design variables corresponding to the maximum EI is fed back into the finite element model for verification. The resulting data are then added to the sample set to achieve dynamic updating and local refinement of the surrogate model.

Convergence Assessment: The process determines whether the current minimum objective value meets the preset accuracy requirements or convergence criteria. If satisfied, the optimal combination of structural parameters is output, and the optimization concludes; otherwise, the iterative process continues.

4. Simulation Results and Analysis

4.1. Comparative Analysis of Harmonic Characteristics

Based on the optimization method described in Chapter 3, an optimal set of structural parameters was ultimately obtained: mover end-tooth thickness ($h_a = 2.1$mm), air gap length ($\delta = 0.45$mm), and slot depth ($h_d = 4.8$mm). At this stage, the objective function reached convergence after 50 iterations of the Efficient Global Optimization (EGO) process, as illustrated in Fig. 5. To systematically evaluate the effectiveness of this optimization scheme, a Fast Fourier Transform (FFT) analysis was performed on the mover's induced electromotive force (EMF) both before and after optimization.

As shown in Fig. 6, the simulation results indicate that prior to optimization, the induced EMF exhibited prominent 3rd, 5th, and 7th spatial harmonics with high amplitudes, leading to a Total Harmonic Distortion (THD) of up to 5.32%. Specifically, the 3rd harmonic primarily stems from the non-sinusoidal distribution of the air gap magnetic field and field distortions caused by longitudinal end effects.

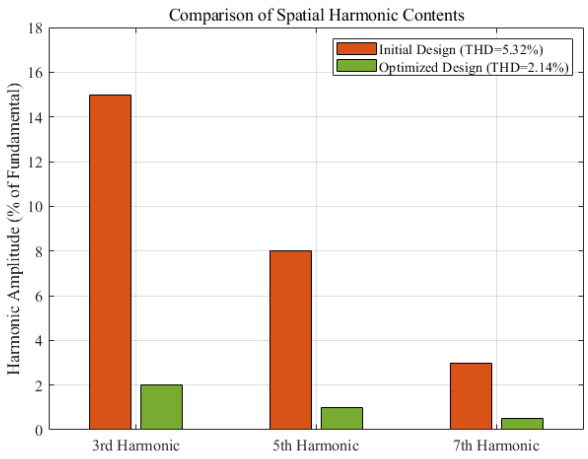

Fig 7. FFT analysis of induced EMF before and after optimization

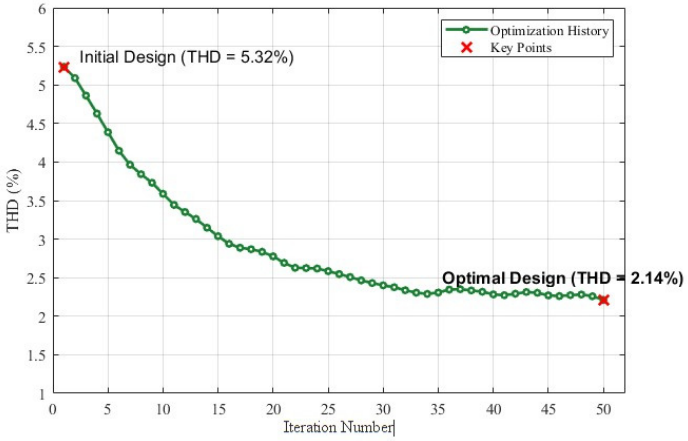

Fig 8. THD iterative optimization process

Post-optimization, by appropriately increasing the mover end-tooth thickness, the end-leakage flux was effectively suppressed and the air gap magnetic flux path was improved. This resulted in an air gap magnetic flux density distribution that more closely approximates an ideal sinusoidal waveform. FFT analysis further demonstrates that the 3rd harmonic amplitude was significantly reduced after optimization, with the total THD dropping to 2.14%—a reduction of 59.8% compared to the initial state. These findings indicate that the proposed optimization method effectively suppresses major harmonic components, significantly enhancing the sinusoidality of the output signal and the position detection accuracy of the system.

4.2. Position Detection Accuracy (Electrical Angle Error)

The reduction in Total Harmonic Distortion (THD) is directly correlated with the enhancement of output signal quality. However, the core metric for evaluating the performance of the Linear Variable Reluctance Resolver (LVRR) lies in its position detection accuracy. To this end, the positioning performance before and after optimization was quantitatively evaluated by calculating the electrical angle error. This error is obtained by comparing the electrical angle decoded from the sensor output voltages with the theoretical electrical angle corresponding to the actual mechanical position of the mover.

Electrical angle error serves as the ultimate benchmark for LVRR performance. By comparing the electrical angle obtained through the arctangent decoding method with the true mechanical position, the error is defined as:

$$\varepsilon = \theta_{elec} - \theta_{mech} = \arctan\left(\frac{u_s}{u_c}\right) - \frac{2\pi x}{\tau} \quad (2)$$

n Equation (2), ε represents the electrical angle error, which is the core metric for evaluating the position detection accuracy of the LVRR; its value directly reflects the linearity of the system. θ_{elec} is the measured electrical angle decoded from the sensor output signals, where u_s and u_c denote the fundamental amplitudes of the induced electromotive forces (EMF) in the sine and cosine phase output windings, respectively. θ_{mech} represents the ground-truth theoretical electrical angle corresponding to the actual mechanical displacement of the mover. Here, x is the real-time displacement of the mover along the direction of motion, and τ is the mover pole pitch, signifying that a mover displacement of one tooth pitch corresponds to an electrical angle change of 2π radians. This equation quantifies the nonlinear deviation of the measured values relative to the theoretical values caused by high-order harmonics of the air gap magnetic field and end effects.

The simulation results are illustrated in Fig. 7. Prior to optimization, the electrical angle error curve exhibited significant high-frequency oscillations, with a peak-to-peak error of ±2.8°. Following the optimization, the smoothness of the curve improved substantially, and high-frequency noise was effectively suppressed, with the maximum electrical angle error converging to within ±0.9°. These results demonstrate a significant enhancement in the positioning accuracy of the linear motor drive system, meeting the rigorous requirements for high-end industrial applications.

5. Conclusion

To address the degradation of position detection accuracy in the Linear Variable Reluctance Resolver (LVRR) caused by its open-circuit structure and end effects, this study proposes an efficient structural optimization design method based on the Kriging surrogate model. The research demonstrates that the established equivalent model clearly elucidates the physical mechanisms of local magnetic saturation and air gap magnetic field distortion induced by end effects. The employed sequential iterative optimization strategy significantly enhances computational efficiency while ensuring global optimization capability[3,10]. The final optimized structure effectively suppresses end-leakage flux, leading to a substantial reduction in both output voltage THD and electrical angle error, with performance fulfilling the requirements for high-precision displacement sensing.

While this study has achieved the expected progress in theoretical modeling and static optimization, several limitations remain. First, the optimization process was primarily based on ideal electromagnetic conditions and did not comprehensively account for the impacts of manufacturing tolerances, assembly errors, or thermal-field coupling on sensor performance. Second, the performance evolution under dynamic operating conditions (such as electromagnetic characteristics at varying speeds, vibration, and dynamic eccentricity) has not been fully explored.

Future work will focus on the following areas:

1.Establishing multiphysics coupling models to conduct robust optimization designs that incorporate manufacturing tolerances and temperature rise effects.

2.Investigating the output characteristics and compensation methods for the LVRR under dynamic operating conditions.

3.Exploring the rapid design of other high-performance linear sensor topologies based on the proposed methodology.

Acknowledgments

This work is supported by National Natural Science Foundation of China (No. 52375270), Henan Natural Science Foundation (No. 262300421012) and Program for Innovative Research Team in Science and Technology of Henan Province (25IRTSTHN023).

References

[1] Torkaman, H., et al. "Reduction of End Effect in Linear Variable Reluctance Resolver." 2024 4th International Conference on Electrical Machines and Drives (ICEMD), 2024.

[2] Li, J., et al. "Data-Driven Surrogate-Assisted Multi-Objective Optimization for Electromagnetic Devices." IEEE Transactions on Magnetics, vol. 58, no. 2, 2022.

[3] Xiao, S., et al. "Kriging-Assisted Topology Optimization of Synchronous Reluctance Machines." IEEE Transactions on Energy Conversion, vol. 36, no. 3, 2021.

[4] Nasiri-Gheidari, Z., et al. "Design Optimization of Linear Variable-Reluctance Resolver for Higher Accuracy and Smaller Size." IEEE Sensors Journal, vol. 23, no. 15, pp. 16543-16552, 2023.

[5] Bahari, M., et al. "Development of a Multiturn Linear Variable Reluctance Resolver With Integrated Ferromagnetic Core." IEEE Transactions on Industrial Electronics, 2024.

[6] Liu, C., et al. "Optimization Design of Variable Reluctance Resolver Based on Three-phase Symmetrical Winding." Machines, vol. 12, no. 5, 2024.

[7] Lasjerdi, H., & Nasiri-Gheidari, Z. "Improving the Performance of Variable Reluctance Resolver Against Short Circuit Using Physical Parameters." Scientia Iranica, 2023.

[8] Wang, Y., et al. "Optimization of Stator Structure for Improved Accuracy in Variable Reluctance Resolvers Using Advanced Machine Learning Techniques." Energies, vol. 17, no. 21, 5454, 2024.

[9] Moghaddam, R. R., et al. "Performance Evaluation of Variable Reluctance Linear Resolver Based on the Hybrid Model Across a Wide Velocity Range." IEEE Conference Publications, 2024.

[10] Zhang, B., et al. "Multi-objective Optimization of Linear Motor Based on Kriging Model and Genetic Algorithm." Proceedings of the CSEE, 2022.